Full-aperture backscatter diagnostics and applications at the Texas Petawatt Laser facility

C. Wang, C. Wagner, G. Dyer, E. Gaul, N. Kandadai, N. Riley, D. Kuk, E. McCary, A. Meadows, I. Pomerantz, M. Spinks, T. Borger, A. Bernstein, M. Donovan, M. Martinez, T. Ditmire, and Bjorn M. Hegelich*

Center for High Energy Density Science, University of Texas, Austin, Texas 78712

**Corresponding author: hegelich@physics.utexas.edu*

Received March 26, 2014; accepted May 3, 2014; posted online October 20, 2014

In this paper, we present the development and application of a full-aperture backscatter diagnostics system at the Texas Petawatt Laser (TPW) facility. The diagnostic system includes three independent diagnostic stations. With this system, we obtained TPW on-shot focus properties, and high-harmonic spectral emission from solid foils (e.g., Cu and Al) and their Si substrate in an experiment to study laser hole boring, which show the hole-boring mechanism at relativistic intensities. The measured on-target full-power focal spots from ultrathin film targets help determine the optimum target thickness at certain laser contrast parameters for particle acceleration and neutron generation experiment, which is also a relative measurement of shot-to-shot intensity fluctuations.

OCIS codes: 320.7090, 020.2649, 300.6360, 350.5400.

DOI: 10.3788/COL201412.S23201.

High-power, ultrafast laser backscatter diagnostics are essential for characterizing the energy and spectrum of scattered light produced by laser–plasma interactions. Such diagnostics have been developed for most large laser facilities, such as the National Ignition Facility[1], the Trident Laser Facility at Los Alamos National Lab[2], and the Shenguang Laser Facility at SIOM[3].

In this paper, we report the development and application of full-aperture backscatter diagnostics at the Texas Petawatt Laser (TPW) facility. This diagnostic includes three independent backscatter diagnostic stations. The TPW is a laser with interaction intensities of $>10^{21}$ W/cm^2 and pulse durations of <150 fs (full width at half maximum, FWHM)[4]. Applying this laser, opens up new potential for producing high-energy particles, including electrons[5,6], protons[7], and neutrons[8] through laser–plasma interactions. Here, we describe this diagnostic and introduce the alignment procedure. We also give an example of applying this diagnostic: the experiment on laser hole boring[9]. In this experiment, we measured the TPW on-shot laser pulse at focus and obtained harmonic spectral emission from the front side of free-standing, solid ultrathin targets (Cu, Ag, and Si). We compared the results from full-energy (~100 J) shots with those from lower-energy (~40J) shots, which shows the hole-boring mechanism at relativistic intensities. We also applied this diagnostic to study the interaction of ultrashort laser pulses with ultrathin, over-dense plastic targets used in electron and proton acceleration, and neutron generation. Using this backscatter technique, we can obtain more information to determine the optimum target thickness at certain laser contrast parameters. Finally, we present our conclusions and describe our future plans on this diagnostic, including time-resolved spectroscopy to investigate the dynamics of target heating and expansion processes, and the transparency or opaqueness of the plasma at peak interaction. This information is key to determine the particle acceleration mechanisms at work and to optimize the interaction with respect to laser and target parameters.

The backscatter diagnostics can capture laser focus information on a foil target and measure generated harmonic spectra from the target in a full-power system shot. Figure 1 is an overview of the diagnostic setup. When the incident TPW laser pulse focuses on a film target, backscattered light from the front surface of the target is collected by an f#/3 off-axis

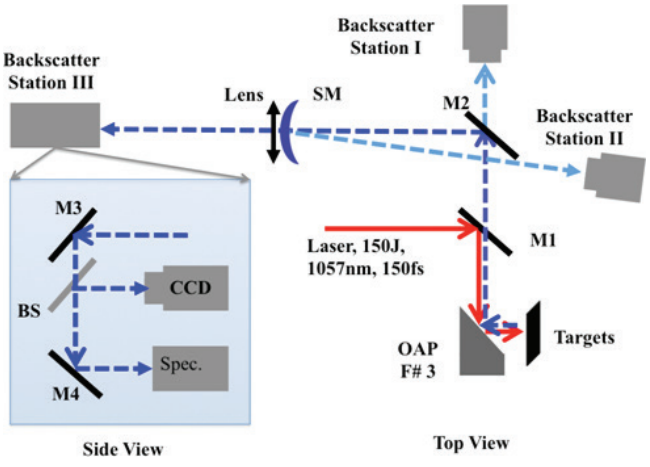

Fig. 1. (Color online) Overview of the backscatter diagnostic experimental setup. Dashed blue lines indicate the backscatter diagnostic optical collection path and solid red lines indicate the main short-pulse laser path. The light blue lines indicate the alternative backscatter diagnostic beam path, where M is mirror. BS, beam splitter; SP, spherical mirror; Spec., spectrometer.

parabolic (OAP) mirror, and it gets collimated with beam diameter of 254-mm. After passing through the mirror M1 inside the laser compressor, the backscattered beam hits on the mirror M2. The transmitted portion of the backscattered beam from M2 is used for Backscatter Station I (as shown in Fig. 1), whereas the reflected portion is further reflected by an f#/40 spherical mirror (SM) and focused to Backscatter Station II. The part of the beam leaking through the spherical mirror is focused by a very long focus lens behind it to the Backscatter Station III in the TPW Laser Bay. Figure 1 also shows a side view of Backscatter Station III. A beam splitter (a wedge) splits the focused backscattered beam to a CCD and a spectrometer for capturing the on-shot laser focus image and backscattered harmonics spectra, respectively. The reflective magnification is ~12×, magnification with lens is ~10×, and all reflective imaging is achromatic.

Alignment of the backscatter diagnostics is crucial to their successful application. To align the backscatter diagnostics, the best focus of the OAP is achieved using an equivalent plane imaging system at target chamber center, based on a microscope objective and a low-power CW or an attenuated optical parametric amplified (OPA) alignment beam. However, this focal-spot characterization method cannot be used on a full-power shot because of the strong thermal effect and *B*-integral effect at laser full power. The backscatter diagnostic allows us to directly measure the actual full-power on-target as-shot focus, which can differ from the low-power measurement[2].

The alignment process is the following: 1) Position microscope objective so as to image best focus from the OAP with CW beam, and switch to attenuated OPA for fine adjustments/focus confirmation. 2) Switch back to CW and pinch the beam to provide a backlight. 3) Move the tip of scanning tunneling microscope (STM) into the correct focal plane (get STM tip in focus through the objective, which had not been moved). 4) Confirm positioning by unpinching the beam. 5) Look at position off scattered light on side-scatter diagnostic, then move the target into the CW beam. When the scattered light off of the target is in the same position as the scattered light from the STM on the side-scatter diagnostic, the target is at the focus of the OAP.

To align the backscatter diagnostics, we use a 532-nm alignment beam to obtain the best image of an object at the OAP focus, such as the STM tip. The 532-nm alignment beam is from a green laser diode mounted in a mirror mount, as shown in Fig. 2(a). The alignment beam passes an STM tip at the OAP focus (tip diameter is ~5-μm) through an optical window of the chamber and arrives at the camera of a backscatter diagnostic. By adjusting the position of the camera, a best-focused tip image can be obtained after the alignment, as shown in Fig. 2(b), which indicates the best position of the camera. By applying certain kinds of glass filters, the backscatter diagnostic allows us to capture backscattered beams at the different wavelengths that are produced in the laser–plasma interaction.

Further, the scale calibration of the camera is achieved by moving the STM tip 150-μm in the focal plane of the OAP, recording images of the STM tip before and after the movement, and calculating pixel differences of the tip position in the two images. We obtained 0.34-nm/pixel for the CCD in focal-spot imaging. The absolute calibrated value of the spectrometer combined with the camera is 0.39 nm/pixel by using Pen-Ray Pare Gas lamps where the spectrometer is microHR Imaging Spectrometer with Basler AF320f camera.

We can align the Backscatter Station III by using the same method we used for Backscatter Station II (Fig. 1). Alternately, if Backscatter Station III is aligned, we can use the image of an STM tip in Backscatter Station II as a reference to align other backscatter stations.

We developed the backscatter diagnostic at a laser hole-boring experiment at TPW and characterized the hole-boring mechanism through this system. The laser hole-boring regime was first numerically simulated by Wilks *et al.*[10]. They found that a laser could bore a hole when irradiated on a solid target if the laser focal-spot size typically is diffraction-limited to about 8 μm, and the laser intensity is sufficient that $I\lambda^2$ is much larger than 10^{18} $\mathrm{Wcm^{-2}\mu m^2}$, where I is the laser intensity and λ the laser center wavelength. Hole-boring results primarily from pressure imbalance:radiation pressure pushes the critical surface into the target, and electrons accumulate in a sheath inside the target, creating charge separation, and when radiation pressure is equal to the pressure exerted by the charge separation, electrons stop acceleration[11,12]. Although hole-boring velocity has been measured by observing the redshift in the reflected hole-boring beam, experimental data on this regime are limited[13].

If we define $\beta = v/c$, where v is the hole-boring velocity and c the speed of light, we have β proportional to $I^{1/2}$ and $n_e^{-1/2}$, where n_e is the target solid density[11]. Because the intensity of TPW is one to two orders of magnitude greater than that used in previous experiments, we are expecting to see an order of magnitude larger hole-boring velocity than that observed in previous experiments[12].

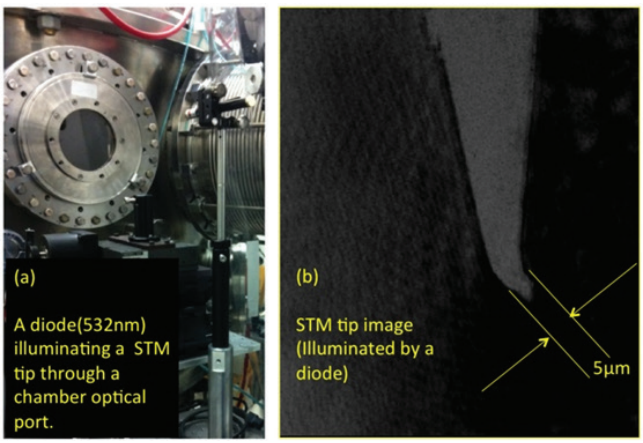

Fig. 2. (Color online) Backscatter Diagnostic III alignment by using a scanning tunneling microscope (STM) tip. (a) A green laser diode (532-nm) illuminates an STM tip at the center of a TPW target chamber, and (b) Forms a sharp focused image at a camera of Backscatter Station III after alignment.

In our experiment, the TPW laser is incident at 22° from the target normal. The targets are Cu, Ag, and their Si substrates. The target thickness is 0.9 and 1.6-μm for Cu, 1-μm for Ag, and 0.5-mm for Si substrate. The through-hole diameter on the Si substrate for fabricating free-standing thin Cu and Ag foils is 1-mm.

The typical on-shot focus image and spectra captured from Backscatter station III are shown in Fig. 3. For this shot, the laser pulse energy at 99 J, pulse duration 150 fs, and center wavelength λ_L = 1057-nm, irradiates a Si substrate at 22° from target normal. Figure 3(a) shows the captured focus of the laser beam on Si slab target by focusing the backscattered visible wavelength range. The focal-spot diameter (FWHM) is larger than 10-μm because we aligned the system by using a green 532-nm beam. The lens behind the spherical mirror may produce chromatic aberration in the captured focus image in a wide backscattered wavelength range. In Fig. 3(b), we can determine the redshifted wavelength of the third-harmonic generation λ_{rf} from the laser–solid film interaction. With λ_{rf}, we then calculate the frequency (or wavelength) that the generated plasma emitted λ_{Sou} from $(\lambda_{Sou} - \lambda_L)/\lambda_L = (\lambda_{rf} - \lambda_L/2)/(2\lambda_L)$. By using the equation $[(1 + \beta)/(1 - \beta)]^{1/2} - 1 = (\lambda_{Obs} - \lambda_{Sou})/\lambda_{Sou}$, we can obtain the value of β. The calculated β from Fig. 3 is 0.2, which shows that the generated plasma by the TPW laser moves about 20% of the speed of light c at this experiment. This very fast recession velocity is probably due to the pre-pulse we have in the laser. The pre-pulse may generate a layer of pre-plasma with densities significantly lower than solid densities that the critical surface of the pre-plasma will be pushed forward much more quickly.

Further measured results on the thin Cu and Ag foils at different laser energies are shown in Fig. 3(c), which indicate the redshifting of the generated second-harmonic beam. The calculated β values at different redshifted wavelengths are listed at the bottom of the x-axis, which shows we may be able to get the hole-boring velocity about 20% of the speed of light even though limited by our spectrometer properties, we did not capture the whole redshifting spectra of second-harmonic beams. For these shots, the energy of the laser changed from ~40 to ~120 J for different targets with the same pulse duration of 150 fs (FWHM). We also measured redshifting of a third-harmonic spectrum by capturing the reflected beam in 10° to the target normal. The results are prepared for publications.

In addition, we have applied this diagnostic to an ultrathin foil experiment for electron and proton acceleration, and neutron generation experiment at TPW, which helps determine the optimum target thickness at certain parameters of the laser system.

In this experiment, we applied very thin plastic films as transparent over-dense targets to have high propagation and high interaction density for laser-induced ion accelerations[14]. For such thin targets, very high laser contrast is required. However, in the high-power ultrashort pulse generation process, because of the nature of chirped pulse amplification process, reflection of optical surfaces, and ghost focuses of lenses in the system, the short high-intensity pulse sits on a nanosecond

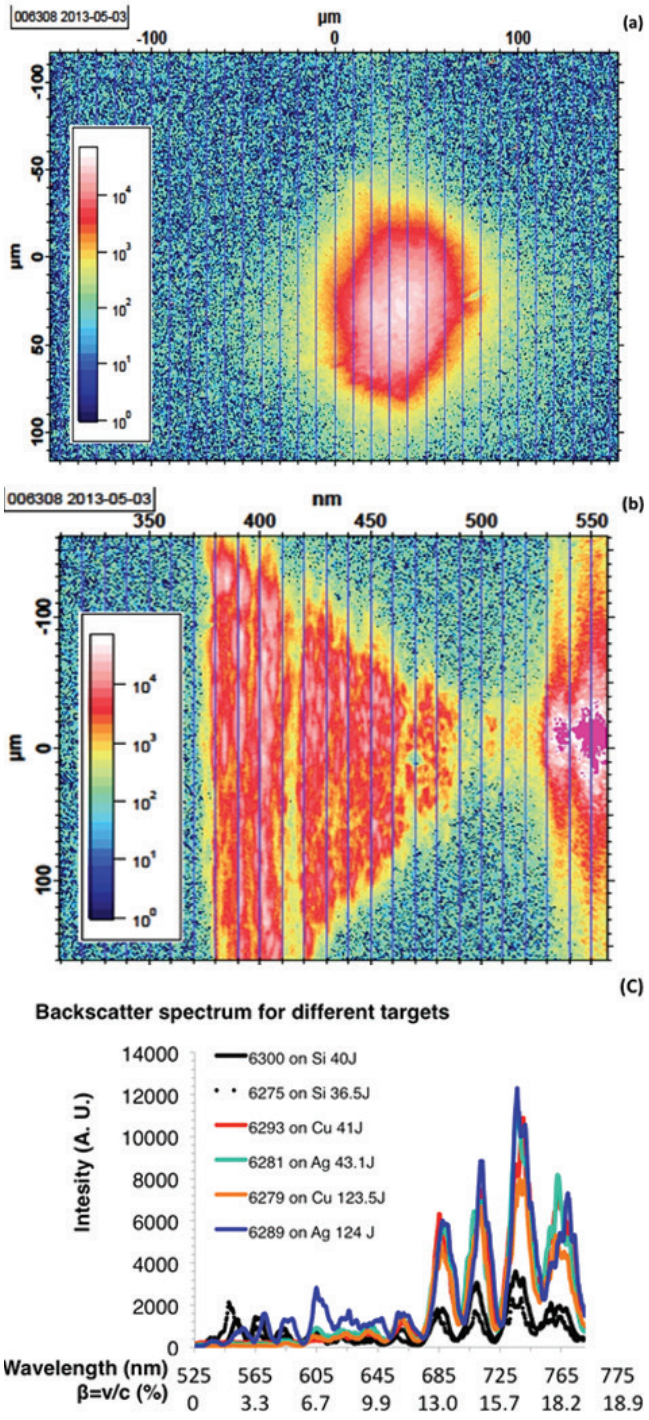

Fig. 3. (Color online) Backscattered on-shot focus image and spectra in a TPW laser hole-boring experiment. (a) Measured on-shot focus image (infrared wavelength filtered by a KG3 glass filter). (b) Measured spectrum from a 0.5-mm-thick Si foil at laser energy of 99 J at blue wavelength range. (c) Measured spectra from Ag (1 μm thick) and Cu (0.9 μm thick) foil at different laser energy at green wavelength range.

pedestal of incompressible noise. The pedestal, or the pre-pulse, often changes the optimum thickness of targets in the experiment[14].

As it is very important to find the optimum thickness for the TPW Laser facility, a bright laser focus image

from a backscatter diagnostic station indicates that the high-intensity laser pulse is actually interacted with an over-dense target, which can narrow down the target thickness ranges. As Fig. 4 shows, in the experiment, the OAP focuses the TPW laser pulse and is incident on thin-film targets in target normal. While the captured backscattered image from a 13-μm plastic film target [as shown in Fig. 4(a)] saturated the camera, the image from a 20-nm polyethylene terephthalate (PET) plastic film [Fig. 4(c)] is much weaker than that from a 300-nm TPX plastic (polymethylpentene) thin film [Fig. 4(b)]. We could not capture any backscatter focus images if the target is too thin to backscatter any light to the diagnostic station. With this, we narrowed down the optimum target thickness range for ion acceleration and neutron generation experiments. This target thickness–dependent backscattered focal-spot information strongly indicates the laser intensity and contrast information during the laser–solid interaction. Our group has submitted the result from this experiment to PRL for review. In addition, if we image the laser–solid film interaction region in third-harmonic order, we could further use the backscatter diagnostic as a more accurate focal-spot diagnostic for high-intensity laser–solid interactions[15].

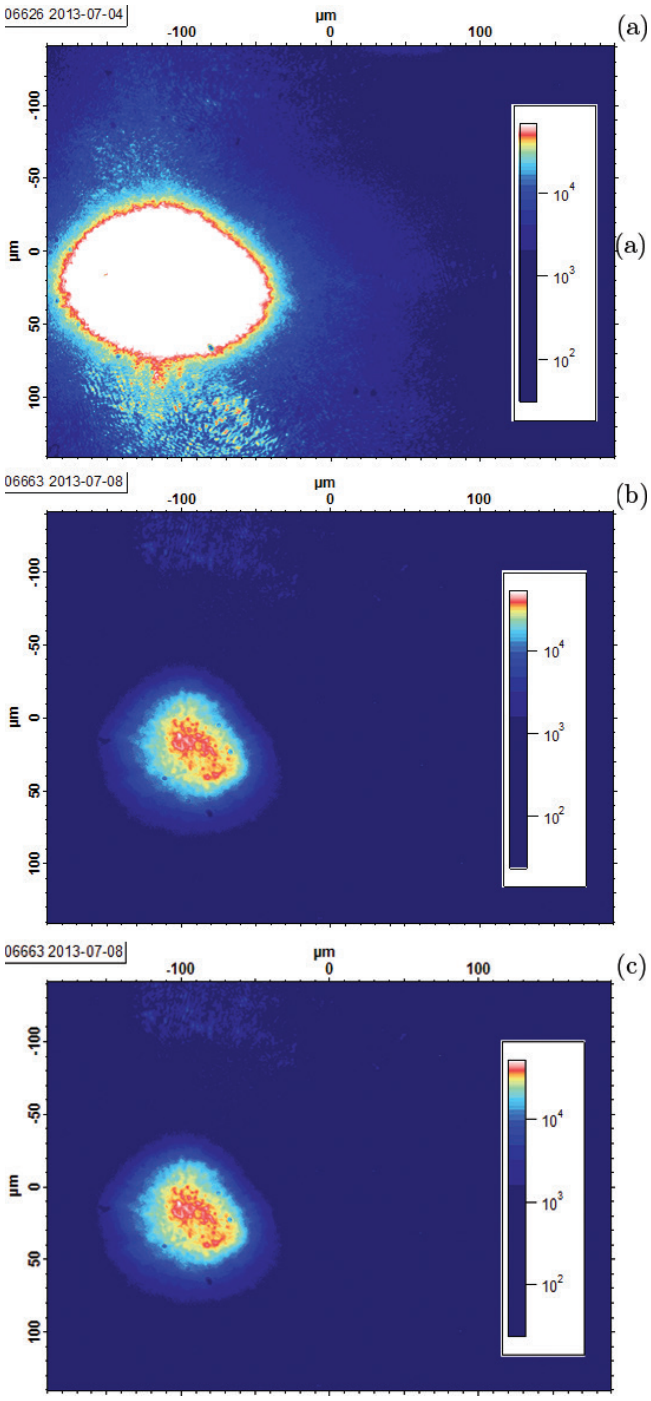

Fig. 4. (Color online) Backscatter focal-spot images from Backscatter Station I on a particle acceleration and neutron generation experiment: (a) 13-μm PMMA plastic film target; (b) a 0.3-μm TPX (polymethylpentene) thin film; and (c) a 0.02-μm PET thin film. The TPW laser is incident on these film targets in target normal with intensities at ~20×10^{20} W/cm^2. Wavelengths longer than 800 nm are filtered away by a KG3 glass filter adding in front of the image camera.

In conclusion, we have developed a full-aperture backscatter diagnostic at the TPW Laser facility and applied it to a TPW laser hole-boring experiment and a laser particle acceleration from a laser–plasma interaction experiment. With this diagnostic, we obtained the laser full-power on-shot focus information and measured the backscattered high harmonic emission from the TPW laser hole-boring experiment on Cu and Ag foils, and their Si substrates. The measured high-harmonic backscattered emission spectra suggest the laser hole-boring velocity could be 20% of the speed of light or larger. This higher velocity is very likely due to the extremely high TPW power (>10^{21} W/cm^2) with very tight focus on a solid foil and the lower density of the pre-plasma created by the laser pre-pulse, which may be pushed forward much more quickly.

As the TPW laser is upgrading to a much high laser intensity contrast, this full-aperture diagnostic could help us determine the optimum target thickness of thin films at certain laser contrast parameters by characterizing the laser full-power on-shot focal spot on target. Because the obtained results are time integrated, in the future, we will focus on developing time-resolved backscatter diagnostics to explore the evolution of the target properties on shot, and the laser-induced target heating and expansion processes. The technologies that we can use include frequency-resolved optical gating technologies for charactering the backscattered beam generated from laser–plasma interaction[16].

The authors appreciate the useful discussions with Sasikumar Palaniyappan, Donard C. Gautier, and Juan C. Fernandez at Los Alamos National Laboratory.

References

1. J. D. Moody, P. Datte, K. Krauter, E. Bond, P. A. Michel, S. H. Glenzer, L. Divol, C. Niemann, L. Suter, N. Meezan, B. J. MacGowan, R. Hibbard, R. London, J. Kilkenny, R. Wallace, J. L. Kline, K. Knittel, G. Frieders, B. Golick, G. Ross, K. Widmann, J. Jackson, S. Vernon, and T. Clancy., Rev. Sci. Instrum. **81**, 10D921 (2010).

2. D. C. Gautier, K. A. Flippo, S. A. Letzring, J. W. Shimada, R. P. Johnson, T. R. Hurry, S. A. Gaillard, and B. M. Hegelich., Rev. Sci. Instrum. **79**, 10F547 (2008).
3. F. Wang, X.-S. Peng, D. Yang, Z.-C. Li, T. Xu, H.-Y. Wei, and S.-Y. Liu, Acta Phys. Sin. **62,** 17 (2013).
4. M. Martinez, W. Bang, G. Dyer, X. Wang, E. Gaul, T. Borger, M. Ringuette, M. Spinks, H. Quevedo, A. Bernstein, M. Donovan, and T. Ditmire, in *15th Advanced Accelerator Concepts Workshop, AIP Conference Proceedings* **1507,** 874 (2012).
5. X. Wang, R. Zgadzaj, N. Fazel, Z. Li, S. A. Yi, X. Zhang, W. Henderson, Y. Y. Chang, R. Korzekwa, H. E. Tsai, C. H. Pai, H. Quevedo, G. Dyer, E. Gaul, M. Martinez, A. C. Bernstein, T. Borger, M. Spinks, M. Donovan, V. Khudik, G. Shvets, T. Ditmire, and M. C. Downer, Nat. Commun. **4,** 1988 (2013).
6. D. Taylor, E. Liang, T. Clarke, A. Henderson, P. Chaguine, X. Wang, G. Dyer, K. Serratto, N. Riley, M. Donovan, and T. Ditmire, High Energy Density Physics **9,** 363 (2013).
7. B. M. Hegelich, I. Pomerantz, L. Yin, H. C. Wu, D. Jung, B. J. Albright, D. C. Gautier, S. Letzring, S. Palaniyappan, R. Shah, K. Allinger, R. Hörlein, J. Schreiber, D. Habs, J. Blakeney, G. Dyer, L. Fuller, E. Gaul, E. Mccary, A. R. Meadows, C. Wang, T. Ditmire, and J. C. Fernandez, New J. Phys. **15,** 085015 (2013).
8. M. Storm, S. Jiang, D. Wertepny, C. Orban, J. Morrison, C. Willis, E. McCary, P. Belancourt, J. Snyder, E. Chowdhury, W. Bang, E. Gaul, G. Dyer, T. Ditmire, R. R. Freeman, and K. Akli, Phys. Plasmas **20,** 053106 (2013).
9. I. V. Pogorelsky, N. P. Dover, M. Babzien, A. R. Bell, A. E. Dangor, T. Horbury, C. A. J. Palmer, M. Polyanskiy, J. Schreiber, S. Schwartz, P. Shkolnikov, V. Yakimenko, and Z. Najmudin, in *Advanced Accelerator Concepts* 814 (2012).
10. S. C. Wilks, W. L. Kruer, M. Tabak, and A. B. Langdon, Phys. Rev. Lett. **69**, 1383 (1992).
11. P. Gibbon, *Short Pulse Laser Interactions with Matter: An Introduction* (Imperial College Press, London, 2005).
12. K. Takahashi, R. Kodama, K. A. Tanaka, H. Hashimoto, Y. Kato, K. Mima, F. A. Weber, T. W. Jr Barbee, L. B. Da Silva, Phys. Rev. Lett. **84**, 2405 (2000).
13. S. Kar, K. F. Kakolee, M. Cerchez, D. Doria, A. Macchi, P. McKenna, D. Neely, J. Osterholz, K. Quinn, B. Ramakrishna, G. Sarri, O. Willi, X. H. Yuan, M. Zepf, and M. Borghesi, Plasma Phys. Control. Fusion **55**, 124030 (2013).
14. B. M. Hegelich, D. Jung, B. J. Albright, J. C. Fernandez, D. C. Gautier, C. Huang, T. J. Kwan, S. Letzring, S. Palaniyappan, R. C. Shah, H.-C. Wu, L. Yin, A. Henig, R. Hörlein, D. Kiefer, J. Schreiber, X. Q. Yan, T. Tajima, D. Habs, B. Dromey, and J. J. Honr, Nucl. Fusion **51**, 083011 (2011).
15. B. Dromey, C. Bellei, D. C. Carroll, R. J. Clarke, J. S. Green, S. Kar, S. Kneipa, K. Markeya, S. R. Nagela, L. Willingalea, P. McKennaa, D. Neelya, Z. Najmudina, K. Krushelnicka, P. A. Norreysa, and M. Zepfa, Laser Part. Beams **27**, 243 (2009).
16. S. Palaniyappan, B. M. Hegelich, H.-C. Wu, D. Jung, D. C. Gautier, L. Yin, B. J. Albright, R. P. Johnson, T. Shimada, S. Letzring, D. T. Offermann, J. Ren, C. Huang, R. Hörlein, B. Dromey, J. C. Fernandez, and R. C. Shah, Nat. Phys. **8**, 763 (2012).